IEEE Photonics Journal
An IEEE Photonics Society Publication

Open Access

Probing the Plasmon Coupling, Quantum Yield, and Effects of Tip Geometry of Gold Nanoparticle Using Analytical Models and FDTD Simulation

Volume 10, Number 3, June 2018

Abu S. M. Mohsin
Mariam B. Salim

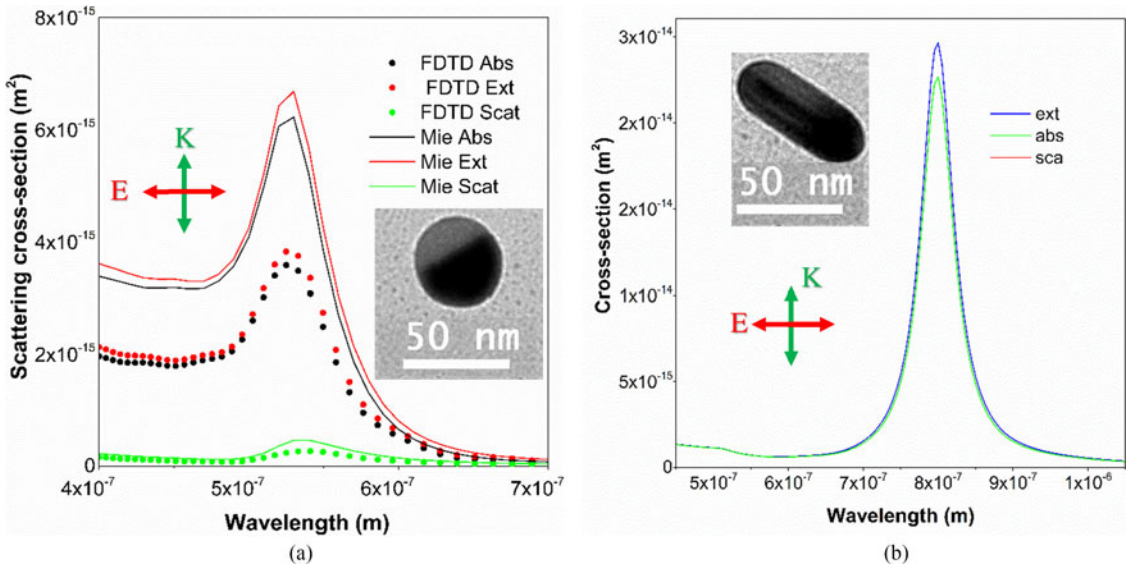

DOI: 10.1109/JPHOT.2018.2825435
1943-0655 © 2018 IEEE

Probing the Plasmon Coupling, Quantum Yield, and Effects of Tip Geometry of Gold Nanoparticle Using Analytical Models and FDTD Simulation

Abu S. M. Mohsin [1] **and Mariam B. Salim**[2]

[1]Centre for Microphotonics, Department of Physics, Faculty of Science, Engineering and Technology, Swinburne University of Technology, Hawthorn VIC 3122, Australia
[2]Faculty of Science, Engineering and Technology, Swinburne University of Technology, Hawthorn VIC 3122, Australia

DOI:10.1109/JPHOT.2018.2825435

Manuscript received March 6, 2018; revised April 3, 2018; accepted April 7, 2018. Date of publication April 12, 2017; date of current version May 23, 2018. Corresponding author: Abu S. M. Mohsin (e-mail: amohsin@swin.edu.au).
This paper has supplementary downloadable material available at http://ieeexplore.ieee.org.

Abstract: In this paper, we investigated the plasmon coupling, quantum yield (QY) and effect of tip geometry of gold nanoparticles (AuNPs) using finite-difference time-domain (FDTD) simulation. Standalone AuNPs spectra have been obtained using the most reliable electromagnetic theory such as Mie theory for spherical nanoparticle such as gold nanosphere (AuNS) and Mie–Gans theory for ellipsoidal AuNPs such as gold nanorod (AuNR). We reported the scattering cross section for standalone and coupling particle using the modified dielectric constant, where the size effect of small particles and the retardation effect of large particles have been taken into consideration for both the analytical calculation and FDTD simulation. Plasmon coupling effect of AuNS dimer of 80-nm diameter and AuNR dimer (side-by-side geometry) of aspect ratio 3.8 has been investigated using FDTD simulation. We also quantified the QY in terms of cluster to monomer ratio for AuNS and AuNR, which is analogous to the ratio of acceptor and donor chromophore in biological systems. The QY of monomer, dimer, and trimer of 40-nm diameter AuNS has been perceived using FDTD simulation, integrating the whole spectrum over 400–1000 nm wavelength regime. Additionally, effect of tip geometry of AuNPs has been investigated and significant field enhancement due to the variation in shapes such as AuNS, AuNR, gold dumbbell, and gold bipyramid has also been reported. The novelty of the paper lies in the presentation of a systematic study of the plasmon coupling of different sizes and shapes of AuNP, quantification of the QY, and probing the effect of tip geometry for a single material such as AuNP using the FDTD simulation. Moreover, we believe that our in-depth analysis of AuNP laid the foundation to determine the scattering cross-section, QY, and near-field enhancement for more complex structures and geometries of other novel materials. Conclusively, the investigation results demonstrate that plasmonic nanoparticle can be used as a molecular probe for bioimaging, sensing, cell signaling, and biological therapeutic intervention.

Index Terms: Gold nanoparticle scattering, Mie theory, Gans theory, nanoparticle plasmon coupling, quantum yield and FDTD simulation.

1. Introduction

Plasmonic nanoparticles exhibit excellent optical properties due to their size, shape and tip geometry. Thus, they have been extensively used in biological applications including biological imaging [1]–[7], bio labelling and sensing [8], photothermal cancer therapy [9], [10], drug and gene delivery [8], [11], and probing membrane proteins [12], [13].

Plasmonic nanoparticle are mediated by localised surface plasmon resonances, which is a charge density oscillations of conduction electrons confined to metallic nanoparticles embedded in dielectric media stimulated by incident light [14]–[19]. The resonance wavelength strongly depends on the size, shape and surface composition of the nanoparticle and the dielectric properties of surrounding medium [16], [19].

Plasmonic nanoparticles (PNPs) exhibit plasmon coupling effect. When two metallic nanoparticles approach each other, a stronger plasmonic near field coupling occurs, giving rise to a distance dependent wavelength shift of the plasmon mode. Quantitative studies on near field coupling between pairs of elliptical metal nanoparticles and spherical nanoparticles as a function of inter particle separation were independently reported by Su [20] and Rechberger [21], respectively. The plasmon coupling effect could be understood using the plasmon hybridisation model, where coupled mode is treated as bonding and antibonding of individual plasmon mode [22]. Recently, PNPs have been exploited to probe inter–particle distances between two macromolecules [13], [23]–[26] utilising the plasmon ruler equation [27], [28] on the basis of spectral shift. Plasmon coupling between a pair of NSs, NRs, nanodisks and nanoshells has been used to detect the DNA–DNA [29]–[31], DNA–protein [32], and protein–protein binary interactions [33]. More recently, plasmon coupling has been utlised to probe the anti–EGFR antibody conjugated PNPs, which has been attached to EGFR protein expressing cells [3], [34].

In recent times, plasmonic nanoparticle has been extensively used in biological applications and it becomes necessity to know the molar absorption, scattering and extinction coefficient or quantum yield. Here, emitting quantum yield is defined as ratio of the aggregate to that of the monomer, which is analogous to the ratio of acceptor and donor chromophore in biological systems. However, quantitative measurement of quantum yield of plasmonic gold nanoparticle will enable us to detect two closely separated molecules [35]–[39], characterise larger protein assemblies, and measure the transport properties, molecular activities and cell membrane protein distribution in living cells [35], [40]. This will provide the solution of measuring slower protein transport which is inaccessible using different microscopy based techniques like Fluorescence resonance energy transfer (FRET) [41], [42], Image correlation microscopy (ICM) [12], [40], Fluorescence correlation spectroscopy (FCS) [43]–[45], and Image correlation spectroscopy (ICS) [46]–[48].

Therefore, to investigate the plasmon coupling, quantify the quantum yield and effect of tip geometry of gold nanoparticles, FDTD simulation has been exploited which has been discussed in the later section.

2. Analytical Models and Numerical Simulation

2.1 Analytical Models

To obtain the single particle spectra, Mie theory is used for spherical nanoparticle such as nanosphere and Mie-Gans theory for ellipsoidal nanoparticle such as nanorod. Mie theory can give the exact analytical solution of a sphere with an arbitrary shape, given that the dielectric constants of the environments are known [49]–[51]. Mie-Gans theory can give the analytical expression to calculate the spectrum for rod shaped (approximated) nanoparticles, which are much smaller than the wavelength of light [14]–[19], [49]–[54]. Due to the absence of analytical models, numerical simulation technique such as discrete dipole approximation (DDA) [55], finite difference time domain (FDTD) [56], [57] or finite element calculations has been used for other shapes.

2.1.1 Extinction of Light by a Nanosphere: In 1908, Gustav Mie proposed a theory for arbitrary shaped spherical particle to solve Maxwell's equation with the correct boundary conditions. This solution can be used to determine the absorption, scattering, and extinction of arbitrary shaped nanoparticles. The cross-section of an arbitrary shaped nanoparticles depends on the radius of

nanosphere R, vacuum number of the incident light K, and dielectric function of the nanospehre ϵ_p and it's surrounding ϵ_m, which has been expressed as,

$$\sigma_{scat} = \frac{2\pi}{k^2}\sum_{n=1}^{\infty}(2n+1)(|a_n|^2+|b_n|^2) \quad \text{and} \quad \sigma_{ext} = \frac{2\pi}{k^2}\text{Re}(a_n+b_n)$$

The coefficient a_n and b_n can be calculated from the following equation

$$a_n = \frac{m\Psi_n(mx)\Psi_n(x) - \Psi_n(mx)\Psi'_n(x)}{m\Psi'_n(mx)\xi_n(x) - \Psi_n(mx)\xi'_n(x)} \quad \text{and} \quad b_n = \frac{\Psi'_n(mx)\Psi_n(x) - m\Psi_n(mx)\Psi'_n(x)}{\Psi'_n(mx)\xi_n(x) - m\Psi_n(mx)\xi'_n(x)}$$

Here, $x = \sqrt{\varepsilon_m}kR$ is a size parameter where R is the radius of the nanosphere, and $m = \sqrt{\frac{\varepsilon_p}{\varepsilon_m}}$ where ε_p and ε_m are the dielectric function of sphere and medium, respectively. Also, ψ and ξ are the Ricatti–Bessel cylindrical function of order n and ψ and ξ and prime indicate differentiation with respect to argument x. The summation of absorbed and scattered energy is known as extinction energy. The phenomenon can be expressed as, $\sigma_{abs} = \sigma_{ext} - \sigma_{scat}$.

Therefore, to calculate the absorption and scattering cross-section, the dielectric function of the particle is required which has been calculated using Drude and Lorentz's free electron models. Dielectric constant of metal is given by the sum of contributions from free electron ϵ_f, (given by Drude's free electron model for metal) and the interband transitions ϵ_{ib}. This yields the following expressions for dielectric constant: $\varepsilon(\omega) = \varepsilon_f(\omega) = +\varepsilon_{ib}(\omega) = 1 - \frac{\omega_p^2}{\omega(\omega+i\gamma_b)} + \varepsilon_{ib}(\omega)$, where ω_p is the plasma frequency and γ_b is the bulk damping constant that is related to the mean free path (l) of the electron through $\gamma_b = v_F/l$, where v_F is the Fermi velocity. The plasma frequency is given by $\omega_p = \sqrt{\frac{ne^2}{\varepsilon_0 m_e}}$, ($\omega_p$ for Au 13.8×10^{15}), where n is the electron density, ε_0 is the vacuum permittivity and m_e is the effective mass of electron.

For small particles (radius less than 5 nm) with dimensions less than the bulk mean free path, the electrons collide with the surface of the particle and the dielectric constant deviates from bulk metal. Considering the electron surface scattering for small particles, the damping constant is given by, $(\gamma_{eff}) = \gamma_b + \frac{A v_F}{l_{eff}}$, where l_{eff} is the effective path length of electrons and A is a constant that depends on the electron–surface interactions [58], [59]. The effective path length depends on the size and shape of the particles and can be calculated consistently for arbitrary shaped particles by $l_{eff} = 4V/S$ where V is the volume of small nanoparticle and S is the surface area of the particle [58], [60]. For spherically capped cylinders (nanorods), effective path length equation becomes $l_{eff} = w\left(1 - \frac{w}{3l}\right)$, where w is the width and l is the total length (l/w is the aspect ratio). For spheres, $l_{eff} = 4/3R$, where R is the radius of sphere and $A_{sphere} = 0.33$. In the case of large particles with a radius above 50 nm, the radiation damping causes broadening of spectrum [14], [18]. If the radiation damping effect is considered, the line width is given by $\Gamma = \gamma_b + \frac{A v_F}{l_{eff}} + 2hkv$, where v is the volume of large nanoparticle and k is a constant that characterises the efficiency of radiation damping. Experimental measurements of dielectric function for Au on metal films under high vacuum [61] are plotted in Supplementary Fig. S1 will be used in all the simulations performed in this paper considering the interband transitions and surface scattering for smaller particles and radiation damping effect for larger particles.

2.1.2 Extinction of Light by a Nanorod: In 1912, Gans developed an extension of Mie's work to calculate the absorption and scattering cross-section of anisotropic particle, where particles much smaller than the wavelength of incident light are approximated as ideal dipoles. The field outside the particles is superposition of ideal dipole and incident field. If an elongated particle is treated as ellipsoid, then its polarizability can be expressed as $\alpha_3 = 4\pi abc\frac{\varepsilon_l - \varepsilon_m}{3\varepsilon_m + 3L_p(\varepsilon_l - \varepsilon_m)}$, where L_p is a depolarisation factor. For prolate spheroids, if light is polarised along the long axis of the spheroids, L_p will change to $L_1 = \frac{1-e^2}{e}\left(-1 + \frac{1}{2e}\ln\frac{1+e}{1-e}\right)$, $L_2 = L_3 = \frac{1-L_1}{2}$, where e is the eccentricity of the particle given by, $e^2 = 1 - (\frac{b}{a})^2$, and $L_p = (L_1, L_2, L_3)$ denotes the polarisation of the incoming field aligned to one of the axes of the particle. The optical cross section can be expressed as $\sigma_{ext} = k/m(\alpha)$ and $\sigma_{sca} = \frac{k^4}{6\pi}|\alpha|^2$.

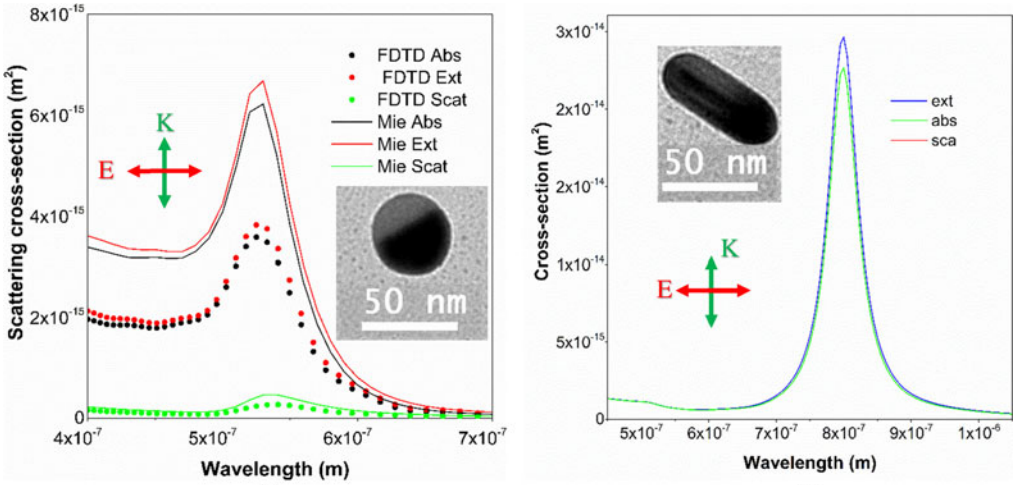

Fig. 1. (a) Extinction, absorption and scattering cross–sections calculated via Mie theory compared with finite difference time domain (FDTD) simulations for 20 nm radius gold nanospheres. (b) Surface plasmon resonance (SPR) spectrum of nanorods with semi major axis 43 nm and semi minor axis 10 nm calculated using Mie–Gans theory, refractive index 1.33. While gold nanospheres show one SPR band in the visible region, gold nanorods show two bands: a strong longitudinal band in the near infrared region corresponding to electron oscillation along the long axis and a weak transverse band, similar to that of gold nanospheres in the visible region corresponding to electron oscillations along the short axis. Inset K vector shows the direction of propagation and E vector shows the direction of electric field considered for FDTD simulation also Transmission Electron Microscopy (TEM) Images of AuNS (Fig. 1(a)) and AuNR (Fig. 1(b)).

In Mie–Gans theory, elongated nanoparticles are approximated as spheroids, however Transmission Electron Microscope (TEM) studies revealed that wet chemically synthesized nanorods have hemispherically capped geometry. Therefore, in our simulation we presumed nanorods as hemispherically capped geometry and corrected the Mie Theory including the geometrical factor (L) for other shape similar to Prescott *et al.* [54]. Moreover, Mie Theory calculated spectra for nanosphere of spherical shape and Mie-Gans Theory calculated spectra for nanorod of hemispherically capped geometry has been compared with similar size and shape FDTD simulated spectra (Fig. 1(a) and (b)). To overcome the shape limitation of analytical model, FDTD simulated has been introduced. Therefore, basic mathematical and physics formalism behind the FDTD algorithm and simulation setup for single AuNPs (monomer) and coupled AuNPs has been presented in the later section.

2.2 Numerical Simulations–FDTD

Recently, different sizes and shapes of PNPs including prisms [62], [63], shells [63], cubes [18], bipyramids [60], and nanorods [15]–[19] have been synthesised and studied optically. Existing analytical models, Mie theory and Mie–Gans theory, only provide the analytical solution of PNP's and infinite long cylinders as special cases [51], however for many other shapes, analytical solutions are not available to investigate the plasmon coupling effect.

The lack of analytical model has set a barrier to understand their plasmon spectra, as well as to gain further insight into their near field properties particularly, the quantum yield of PNPs. Several state of the art methods have been employed to solve Maxwell's equation numerically, including the T–matrix [64], [65], discrete dipole approximation (DDA) [66], and finite difference time domain (FDTD) [57], [66]. The T-matrix method emphasises more on far field properties (i.e., the scattered field) and it is better developed for revolution symmetry. The DDA and FDTD however can give both the near and far field properties due to their finite element nature. However, in this study FDTD

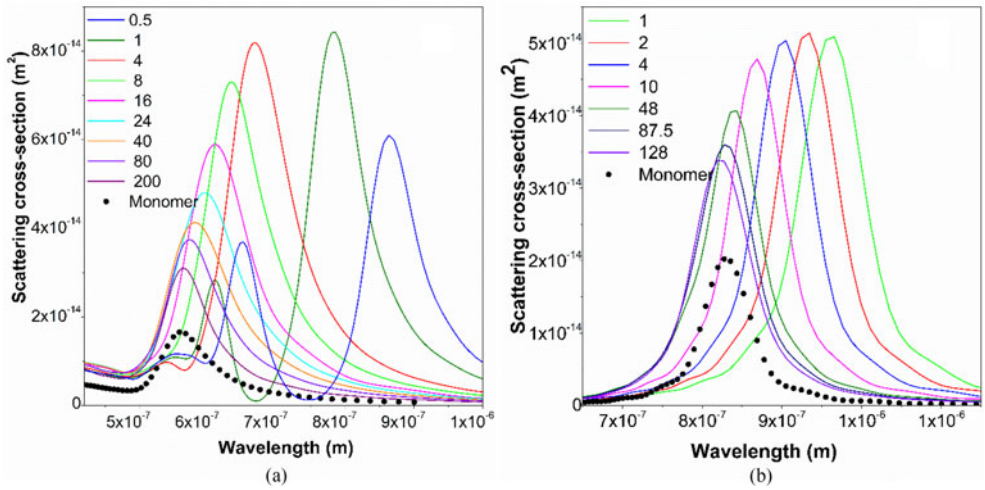

Fig. 2. (a) Finite difference time domain (FDTD) simulation results of 40 nm radius gold nanosphere dimer for 0.5 nm, 1 nm, 4 nm, 8 nm, 16 nm, 24 nm, 40 nm, 80 nm and 200 nm separation compared with monomer. (b) Finite difference time domain (FDTD) simulation results of gold nanorod dimer for length 75 nm, width 20 nm, aspect ratio 3.8, for the separation of 1 nm, 2 nm, 4 nm, 10 nm, 48 nm, 87.5 nm 128 nm compared with monomer.

simulation has been used to explore the coupling effect, quantum yield and effect of tip geometry of different sizes and shapes of AuNS, AuNR, and gold bipyramid and gold dumbbell structures.

2.2.1 FDTD Simulations of AuNS Dimer: To explore the plasmon coupling of AuNP dimer, commercial FDTD software (Lumerical Solutions 7.5, Canada) was used. The dielectric function of gold was formulated from Johnson and Christy has been corrected for size effect (surface scattering and radiation damping). A total- field scattered field source (TFSF) with its wavelength ranging from 400 nm–1000 nm was used and a grid resolution of 0.5 nm was chosen to obtain more accurate results. The source direction was set along the axis of AuNPs. The surrounding medium was taken as water with refractive index 1.33. We investigated the plasmon coupling of 80 nm diameter AuNP dimer using FDTD simulation (Fig. 2(a)) and found red shift in SPR peak with decreasing inter–particle distance (weak coupling region), which is in agreement with previously obtained results [20], [28], [67], [68]. The red shift is due to coupling of plasmonic near field when two spheres approach each other and form bonding and antibonding plasmon modes. Additionally, the amount of red shift is modelled with a universal plasmon ruler equation $\frac{\Delta\lambda}{\lambda} = A \exp - \frac{d/D}{\tau}$, where A = 1.13252 is the maximum fractional plasma resonance shift, $\tau = 0.22513$ is the decay constant, d is the inter–particle separation, and D is the diameter of 80 nm diameter AuNSs (Supplementary Fig. S2). The values have been found to be comparable to published results by Kat *et al.* and Funston *et al.* [27], [28]. There are single SPR peak for weak coupling region, however we found multiple SPR peaks at strong coupling regions specially when the separation is 1 nm or lesser (for 80 nm diameter AuNSs) (Fig. 2(a)). The multiple peak at strong coupling region is due to hybridisation of plasmon energy which could be explained using plasmon excitation model [71]. Moreover, the phase shift is negative, and a sudden fall occurred in phase shift due to the distribution of incident filed energy. In addition to the classical electromagnetic theory, which is the main theoretical framework used in this manuscript, a quantum plasmonic theory is recently being considered a lot especially when the inter-particle distance is below 1 nm. The quantum tunnelling effect may quench the plasmon resonance in the far-field spectrum and consequently the near-field enhancement is reduced a lot. Nevertheless, at weak coupling regions (such as 80 nm and 200 nm separations, respectively), the SPR peak is almost at the same position as monomer SPR peak (around 558 peak wavelengths for 80 nm diameter AuNSs) with double intensity. Intensity of monomer at 558 nm peak wavelength for 80 nm diameter AuNSs is 1.656×10^{-14} m^2. At monomer peak wavelength of 558 nm, the in-

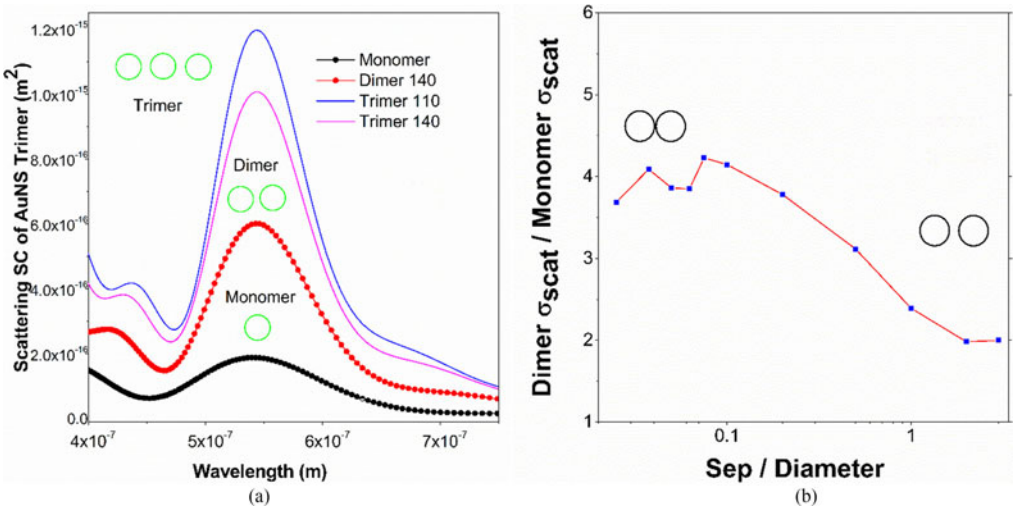

Fig. 3. (a) Finite difference time domain (FDTD) simulation results of 40 nm diameter gold nano sphere trimer for different inter–particle distances for weakly coupling regimes compared with monomer and dimer. (b) Finite difference time domain simulations and quantum yield of 80 nm diameter gold nanosphere (AuNSs) with respect to separation/diameter.

tensity of dimer (8.41×10^{-14} m^2) becomes 5 times greater than the monomer (1.66×10^{-14} m^2) intensity.

2.2.2 FDTD Simulations of AuNR Dimer: Similarly, we simulated spherically capped nanorod dimer with a length of 75 nm, width of 20 nm and aspect ratio 3.8, with side-side geometry and polarisation parallel to long axis (Fig. 2(b)). As the distance decreases, the longitudinal plasmon band progressively red-shifts due to coupling of longitudinal plasmons. The amount of red shift is modelled with the universal plasmon ruler equation, where the results $A = 0.18396$, $\tau = 0.08976$ for aspect ratio (AR) 3.8 has been found to be comparable to published results [27], [28] (Supplementary Fig. S3). However, Funston *et al*. [69] showed that the fitting parameter in universal plasmon ruler equation is not good enough for predicting the coupled plasmon wavelengths of various Au nanorod dimers. In order to have more universal equation, Jain *et al*. [70] reported that coupled plasmon energy is determined by competition between the interparticle coloumbic restoring force on the displaced electron cloud. The d/D term in plasmon ruler equation was replaced by Jiang fang group as $(V_{gap}/V_{nanorod})^{1/3}$, where V_{gap} and $V_{nanorod}$ denote the volumes of the gap region and nanorod respectively. The exponential expression can be articulated as $\frac{\Delta\lambda}{\lambda} = A \exp - \frac{d/D^{1/C}}{\tau}$, where $c = 3, 5$, 7 are for dipole, quadrupole, octupole respectively. To elucidate the nature of plasmon excitation in the coupled system, an excitation model could be employed [71]. For side–side dimer arrangement, longitudinal plasmon bonding is analogous in nature to the formation of σ bond from two P_z electronic orbitals. On the other hand, for side–side dimer arrangement, longitudinal plasmon has anti- bonding in nature which is analogous to the formation of $\pi*$ bond from $P_{x/y}$ orbitals. In the case of end–end dimer configuration, a new band emerges at higher energies as the inter–AuNR distance becomes very small or when the number of AuNRs interacting in assembly is increased [71].

2.2.3 FDTD Simulations of AuNS Trimer: We investigated the plasmon coupling of a nanosphere trimer with a diameter of 40 nm, as a function of interparticle separations (Fig. 3(a)). When comparing the monomer, dimer, and trimer nanospheres with same diameters, it was observed that the peak position remains the same for weakly coupled trimers, dimers and monomers. However, the intensity doubles and triples for dimers and trimers, respectively, due to formation of bonding and antibonding plasmon mode. The intensity and SPR peaks for monomers are 1.89×10^{-16} m^2 and 543 nm, for dimers are 6.01×10^{-16} m^2 and 543 nm, and for trimers are 1.01×10^{-15} m^2 and 543 nm. Plasmon resonance peak shift as a function of inter–particle separations are presented in Supplementary Fig. S4.

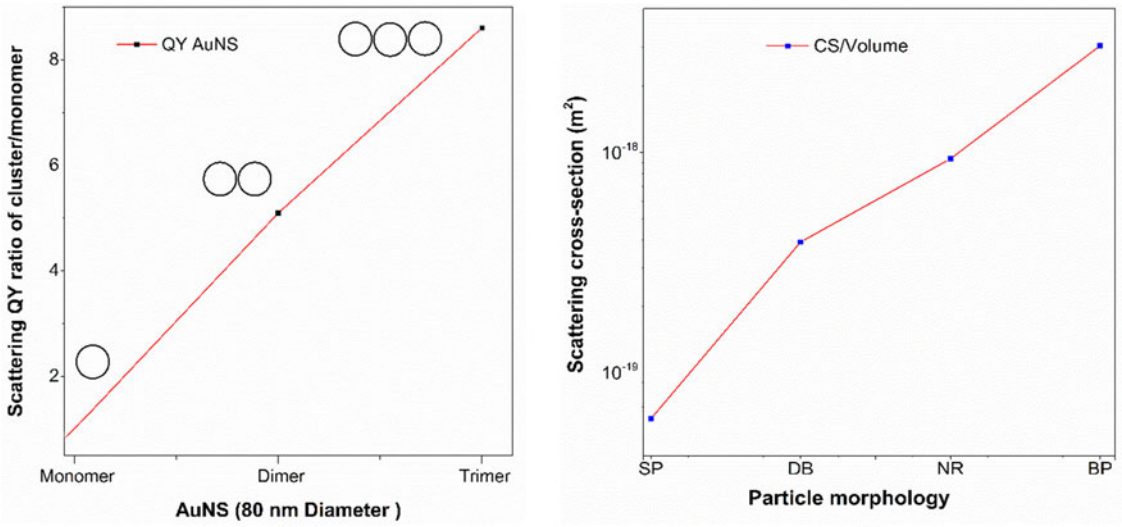

Fig. 4. (a) Extracted Quantum Yield (QY) of AuNP monomer/cluster using FDTD simulation. (b) Scattering cross–sections (per unit volume) of spheres (SPs), dumbbells (DBs), nanorods (NRs) and bipyramids (BPs) using FDTD calculations.

3. Probing Quantam Yield (QY) of Gold Nanoparticle

Quantum yield of AuNPs drastically varies due to plasmon coupling. By simulating PNP plasmon coupling, we can extract the quantum yield ratio of cluster to monomer. Whenever two nanoparticles are brought close together, the plasmon resonance red shifts, and if their separation distance is further reduced, multiple peaks will form due to higher order mode and band splitting. We investigated the plasmon coupling effect of nanospheres and nanorods using FDTD simulation (Fig. 2(a) and (b)). From the FDTD simulation, it was observed that, for 80 nm diameter AuNS, monomers produced SPR peak and scattering intensity of 558 nm and $1.65571 \times 10^{-14}\,m^2$, dimers (1 nm separation) produced SPR peak and scattering intensity of 785 nm and $8.43 \times 10^{-14}\,m^2$, and trimers (1 nm separation) produced SPR peak and scattering intensity of and 877 nm and $1.42 \times 10^{-13}\,m^2$. For AuNR with an aspect ratio of 3.8 nm and length of 75 nm, the SPR peak and scattering intensity for monomers and dimers were 827 nm and $2.02 \times 10^{-14}\,m^2$ and 965 nm and $5.08 \times 10^{-14}\,m^2$, respectively. Furthermore, the total scattering strength of two interacting AuNPs (80 nm diameter AuNS and 3.8 aspect ratio AuNRs) can be calculated by integrating the entire spectrum over 400 nm–1000 nm wavelength regime (Fig. 3(b)). By observing the total scattering strength with respect to separation distance, it can be concluded that whenever two particles are further apart, there is no plasmon coupling & total scattering strength doubles as they act as identical monomers (Fig. 3(b)). From these observations, we can safely assume that for 80 nm diameter AuNS dimers, the QY ratio of the cluster to monomer is around 4, which is the square of the dimer. Similarly, quantum yield ratio of AuNS trimer to AuNS monomer varies from 4 to 9 for different separations, which is cubed for trimer (Fig. 4(a)).

4. Field Enhancement Due to Tip Geometry

Elongated nanoparticles, especially nanorods and bipyramids are promising for optical studies as their spectra are easily tuneable by varying the aspect ratio. Compared with AuNSs, AuNR structures of the same volume give a larger curvature at the tips (Supplementary Fig. S5). Therefore, to investigate the significant field enhancement due to tip curvature, FDTD simulations for AuNS, AuNR, AuDB and AuBP have been performed and their strength has been shown in Fig. 4(b). Gold nanosphere of 80 nm diameter gave a longitudinal plasmon resonance at 2.21 eV (560 nm).

FDTD simulation of AuBP with radius R (radius at equator) = 15 nm, h (total length) = 162 nm and r (radius at poles) = 10 nm dog bone like AuNRs (dumbbells) were also modelled as a cylinder in the middle with two larger spheres at both ends, having a total length of 84 nm and sphere radius of 15 nm. The simulations were performed with 0.5 nm grid resolution and gave a longitudinal plasmon resonance at 1.39 eV (890 nm) and 1.54 eV (805 nm) for AuBP and AuDB respectively. Therefore, scattering spectrum of the above-mentioned diameter is normalized as per unit volume, where AuBP displayed the highest scattering intensity per unit volume while the AuNS yields the lowest scattering intensity. In addition, AuNR produced the second highest scattering intensity per unit volume and AuDB produced the second lowest scattering intensity per unit volume which can be represented as seen in the following sequence AuNS $<$ AuDB $<$ AuNR $<$ AuBP (Fig. 4(b)). A significant field enhancement is observed as AuNRs and AuBPs exhibit around one to three orders of magnitude higher in cross-section than AuNSs (Fig. 4(b)).

5. Conclusion

In this study, we investigated the single particle spectrum such as absorption, extinction, and scattering cross-section of AuNP from 5 nm–100 nm using analytical models Mie Theory and compared the results with simulation technique FDTD. We modified the dielectric constant to consider the size effect of small particles and the retardation effect of large particles for both the analytical calculation and FDTD simulation.

Plasmon coupling effect and quantum yield of spherical gold nanosphere dimer of 80 nm diameter and spherically capped gold nanorod dimer (side-by-side geometry) with aspect ratios of 3.8 has been investigated using FDTD simulation. For AuNS and AuNR dimers (side-by-side geometry), it was found that a decrease in separation distance between adjacent nanoparticles will prompt the plasmon resonance to red shift. Furthermore, greater reduction in the separation distance between adjacent nanoparticles produces multiple SPR peaks that are perceived to be due to higher order mode and band splitting. In addition to finding the plasmon coupling, significant field enhancement due to differences in tip curvature for AuNS, AuNR, AuDB, and AuBP has shown that scattering intensity per unit volume produced the following sequence AuNS $<$ AuDB $<$ AuNR $<$ AuBP where AuNS provided the least scattering intensity per unit volume while AuBP provided the highest. We also investigated the quantum yield of gold nanosphere and found that the quantum yield ratio of the cluster to monomer is about 4. The scattering intensity of the AuNS dimer is increased by power of two over AuNS monomer. Moreover, the quantum yield ratio of a AuNS trimer to AuNS monomer varies from 4 to 9 (for different separation distances) where the scattering intensity is increased by power of three. The novelty of this paper lies in the presentation of a systematic study of plasmon coupling of different sizes and shapes of AuNPs, quantification of quantum yield, and in the investigation of the effect of tip geometry using FDTD simulation. These parameters have been investigated to obtain an in-depth and systematic analysis for one of the most important materials – AuNP, which has not been reported previously. To conclude, we believe that, our results could lead to further developments in the fields of biomedical imaging, sensing, disease diagnosis, drug delivery, photothermal cancer therapy, and optical data storage.

References

[1] P. Zijlstra, J. W. Chon, and M. Gu, "Five-dimensional optical recording mediated by surface plasmons in gold nanorods," *Nature*, vol. 459, no. 7245, pp. 410–413, 2009.
[2] K. Sokolov *et al.*, "Real-time vital optical imaging of precancer using anti-epidermal growth factor receptor antibodies conjugated to gold nanoparticles," *Cancer Res.*, vol. 63, no. 9, pp. 1999–2004, 2003.
[3] J. Aaron *et al.*, "Dynamic imaging of molecular assemblies in live cells based on nanoparticle plasmon resonance coupling," *Nano Lett.*, vol. 9, no. 10, pp. 3612–3618, 2009.
[4] J. Aaron *et al.*, "Plasmon resonance coupling of metal nanoparticles for molecular imaging of carcinogenesis in vivo," *J. Biomed. Opt.*, vol. 12, no. 3, 2007, Art. no. 034007.

[5] I. H. El-Sayed, X. Huang, and M. A. El-Sayed, "Surface plasmon resonance scattering and absorption of anti-EGFR antibody conjugated gold nanoparticles in cancer diagnostics: applications in oral cancer," *Nano Lett.*, vol. 5, no. 5, pp. 829–834, 2005.
[6] R. Mercatelli *et al.*, "Quantitative measurement of scattering and extinction spectra of nanoparticles by darkfield microscopy," *Appl. Phys. Lett.*, vol. 99, no. 13, 2011, Art. no. 131113.
[7] Q. Zhan *et al.*, "A study of mesoporous silica encapsulated gold nanorods as enhanced light scattering probes for cancer cell imaging," *Nanotechnology*, vol. 21, no. 5, 2005, Art. no. 055704.
[8] C. J. Murphy *et al.*, "Chemical sensing and imaging with metallic nanorods," *Chem. Commun.*, no. 5, pp. 544–557, 2008.
[9] X. Huang *et al.*, "Cancer cell imaging and photothermal therapy in the near-infrared region by using gold nanorods," *J. Amer. Chem. Soc.*, vol. 128, no. 6, pp. 2115–2120, 2006.
[10] A. Wijaya *et al.*, "Selective release of multiple DNA oligonucleotides from gold nanorods," *ACS Nano*, vol. 3, no. 1, pp. 80–86, 2008.
[11] C.-C. Chen *et al.*, "DNA-gold nanorod conjugates for remote control of localized gene expression by near infrared irradiation," *J. Amer. Chem. Soc.*, vol. 128, no. 11, pp. 3709–3715, 2006.
[12] A. H. Clayton *et al.*, "Ligand-induced dimer-tetramer transition during the activation of the cell surface epidermal growth factor receptor-A multidimensional microscopy analysis," *J. Biol. Chem.*, vol. 280, no. 34, pp. 30392–30399, 2005.
[13] C. Sönnichsen *et al.*, "A molecular ruler based on plasmon coupling of single gold and silver nanoparticles," *Nature Biotechnol.*, vol. 23, no. 6, pp. 741–745, 2005.
[14] U. V. Kreibig, "Optical sizing of immunolabel clusters through multispectral plasmon coupling microscopy," in *Optical Properties of Metal Clusters*, Berlin, Germany: Springer-Verlag, 1995, pp. 1–436.
[15] P. Mulvaney, "Surface plasmon spectroscopy of nanosized metal particles," *Langmuir*, vol. 12, no. 3, pp. 788–800, 1996.
[16] K. L. Kelly *et al.*, "The optical properties of metal nanoparticles the influence of size shape and dielectric environment," *J. Phys. Chem. B*, vol. 107, no. 3, pp. 668–677, 2003.
[17] X. Lu *et al.*, "Chemical synthesis of novel plasmonic nanoparticles," *Annu. Rev. Phys. Chem.*, vol. 60, no. 1, pp. 167–192, 2009.
[18] Y. G. Sun and Y. N. Xia, "Shape controlled synthesis of gold and silver nanoparticles," *Science*, vol. 298, pp. 2176–2179, 2002.
[19] S. Link, M. B. Mohamed, and M. A. El Sayed, "Simulation of the optical absorption spectra of gold nanorods as a function of their aspect ratio and the effect of the medium dielectric constant," *J. Phys. Chem. B*, vol. 103, no. 16, pp. 3073–3077, 1999.
[20] K. H. Su *et al.*, "Interparticle coupling effects on plasmon resonances of nanogold particles," *Nano Lett.*, vol. 3, no. 8, pp. 1087–1090, 2003.
[21] W. Rechberger *et al.*, "Optical properties of two interacting gold nanoparticles," *Opt. Commun.*, vol. 220, pp. 137–141, 2003.
[22] P. Nordlander *et al.*, "Plasmon hybridization in nanoparticle dimers," *Nano Lett.*, vol. 4, no. 5, pp. 899–903, 2004.
[23] R. Elghanian *et al.*, "Selective colorimetric detection of polynucleotides based on the distance-dependent optical properties of gold nanoparticles," *Science*, vol. 277, no. 5329, pp. 1078–1081, 1997.
[24] A. P. Alivisatos *et al.*, Organization of 'nanocrystal molecules' using DNA, *Nature*, vol. 382, pp. 609–611, 1996.
[25] B. M. Reinhard *et al.*, "Calibration of dynamic molecular rulers based on plasmon coupling between gold nanoparticles," *Nano Lett.*, vol. 5, no. 11, pp. 2246–2252, 2005.
[26] P. K. Jain, W. Huang, and M. A. El-Sayed, "On the universal scaling behavior of the distance decay of plasmon coupling in metal nanoparticle pairs: a plasmon ruler equation," *Nano Lett.*, vol.. 7, no. 7, pp. 2080–2088, 2007.
[27] C. W. Kat *et al.*, "Observation of the fano resonance in gold nanorods supported on high-dielectric-constant substrates," *Acs Nano*, vol. 5, no. 7, pp. 5976–5986, 2011.
[28] A. M. Funston *et al.*, "Coupling modes of gold trimer superstructures," *Phil Trans. Royal Soc. A*, vol. 369, pp. 3472–3482, 2011.
[29] P.-C. Li *et al.*, "Photoacoustic imaging of multiple targets using gold nanorods," *IEEE Trans. Ultrason. Ferroelect. Freq. Control*, vol. 54, no. 8, pp. 1642–1647, Aug. 2007.
[30] G. Decher, "Fuzzy nanoassemblies: toward layered polymeric multicomposites," *Science*, vol. 277, no. 5330, pp. 1232–1237, 1997.
[31] F. Caruso *et al.*, "2. Assembly of alternating polyelectrolyte and protein multilayer films for immunosensing," *Langmuir*, vol. 13, no. 13, pp. 3427–3433, 1997.
[32] D. I. Gittins and F. Caruso, "Tailoring the polyelectrolyte coating of metal nanoparticles," *J. Phys. Chem. B*, vol. 105, no. 29, pp. 6846–6852, 2001.
[33] H. Ai *et al.*, "Electrostatic layer-by-layer nanoassembly on biological microtemplates: platelets," *Biomacromolecules*, vol. 3, no. 3, pp. 560–564, 2002.
[34] H. Wang *et al.*, "Optical sizing of immunolabel clusters through multispectral plasmon coupling microscopy," *Nano Lett.*, vol. 11, no. 2, pp. 498–504, 2011.
[35] J. Aaron *et al.*, "Dynamic imaging of molecular assemblies in live cells based on nanoparticle plasmon resonance coupling," *Nano Lett.*, vol. 9, no. 10, pp. 3612–3618, 2009.
[36] M. J. Crow *et al.*, "Monitoring of receptor dimerization using plasmonic coupling of gold nanoparticles," *ACS Nano*, vol. 5, no. 11, pp. 8532–8540, 2011.
[37] C. Sonnichsen, M. L. ReinhardBjorn, and A. P. Jan Alivisatos, "A molecular ruler based on plasmon coupling of single gold and silver nanoparticles," *Nat. Biotechnol.*, vol. 23, no. 6, pp. 741–745, 2005.
[38] H. Wang *et al.*, "Optical sizing of immunolabel clusters through multispectral plasmon coupling microscopy," *Nano Lett.*, vol. 11, no. 2, pp. 498–504, 2011.
[39] B. M. Reinhard *et al.*, "Calibration of dynamic molecular rulers based on plasmon coupling between gold nanoparticles," *Nano Lett.*, vol.. 5, no. 11, pp. 2246–2252, 2005.

[40] R. B. Ian, W. W. Paul, and W. H. John, "Investigating membrane protein dynamics in living cells this paper is one of a selection of papers published in this Special Issue, entitled CSBMCB–Membrane Proteins in Health and Disease," *Biochem. Cell Biol.*, vol. 84, no. 6, pp. 825–831, 2006.
[41] A. J. E. Elizabeth and M. J. Thomas, "Imaging molecular interactions in living cells by \ FRET\ microscopy," *Current Opinion Chem. Biol.*, vol. 10, no. 5, pp. 409–416, 2006.
[42] Y. T. Roger, J. B. Brian, and R. A. Stephen, "FRET for studying intracellular signalling," *Trends Cell Biol.*, vol. 3, no. 7, pp. 242–224, 1993.
[43] N. O. Peterson, "Scanning fluorescence correlcation spectroscopy. I. Theory and simulation of aggregation measuremets," *Biophys. J.*, vol. 49, pp. 809–815, 1986.
[44] S. Konstantin *et al.*, "Applications of fluorescence correlation spectroscopy: Polydispersity measurements," *J. Colloid Interface Sci.*, vol. 213, no. 2, pp. 479–487, 1999.
[45] N. L. Thompson, "Fluorescence correlation spectroscopy," in *Topics in Fluorescence Spectroscopy: Techniques*, J. R. Lakowicz Ed. New York, NY, USA: Plenum, 1991. p. 1.
[46] N. O. Peterson *et al.*, "Analysis of membrane protein cluster densities and sizes in situ by image correlation spectroscopy," *Faraday Discuss.*, vol. 111, pp. 289–305, 1998.
[47] G. P. Arthur and L. T. Nancy, "Fluorescence correlation spectroscopy for detecting submicroscopic clusters of fluorescent molecules in membranes," *Chem. Phys. Lipids*, vol. 50, no. 3-4, pp. 253–270, 1989.
[48] A. G. Palmer and N. L. Thompson, "High-order fluorescence fluctuation analysis of model protein clusters," *Proc. Nat. Acad. Sci. USA*, vol. 86, no. 16, pp. 6148–6152, 1989.
[49] G. Mie, "Beitrage zur optik truber medien, speziell kolloidaler metallosungen," *Annalen der Physik*, vol. 330, no. 3, pp. 377–445, 1908.
[50] M. Hartmann, "Light Scattering by Small Particles. Von H. C. VANDE HULST. New York: Dover Publications, Inc. 1981," *Acta Polymerica*, vol. 35, no. 4, pp. 338–338, 1984.
[51] C. F. Bohren and D. R. Huffman, "Absorption and scattering of light by small particles," *Research Supported by the University of Arizona and Institute of Occupational and Environmental Health*. New York, NY, USA: Wiley-Intersci., 1983, pp. 1–541.
[52] X. Huang, S. Neretina, and M. A. El Sayed, "Gold nanorods from synthesis and properties to biological and biomedical applications," *Adv. Mater.*, vol. 21, pp. 4880–4910, 2009.
[53] B. Yan and Y. Wang, "Comment on simulation of the optical absorption spectra of gold nanorods as a function of their aspect ratio and the effect of the medium dielectric constant," *J. Phys. Chem. B*, vol. 107, no. 34, pp. 9159–9159, 2003.
[54] S. W. Prescott and P. Mulvaney, "Gold nanorod extinction spectra," *J. Appl. Phys.*, vol. 99, no. 12, 2006, Art. no. 123504.
[55] B. T. Draine and P. J. Flatau, "Discrete dipole approximation for periodic targets theory and tests," *Opt. Soc. Amer. A*, vol. 25, pp. 2693–2703, 2008.
[56] K. Yee, "Numerical solution of initial boundary value problems involving Maxwell's equations in isotropic media," *IEEE Trans. Antennas Propag.*, vol. 14, no. 3, pp. 302–307, May 1966.
[57] A. Taflove and S. C. Hagness, *Computational Electrodynamics the Finite Difference Time Domain Method*. Boston, MA, USA: Artech House, 2000.
[58] E. A. Coronado and G. C. Schatz, "Surface plasmon broadening for arbitrary shape nanoparticles: A geometrical probability approach," *J. Chem. Phys.*, vol. 119, no. 7, pp. 3926–3934.
[59] U. Kreibig and L. Genzel, "Optical absorption of small metallic particles," *Surf. Sci.*, vol. 156, pp. 678–700, 1985.
[60] M. Liu and P. Guyot-Sionnest, "Mechanism of Silver(I)-Assisted growth of gold nanorods and bipyramids," *J. Phys. Chem. B*, vol. 109, no. 47, pp. 22192–22200, 2005.
[61] P. B. Johnson and R. W. Christy, "Optical constants of the noblemetals," *Phys. Rev. B*, vol. 6, no. 12, 1972, Art. no. 4370.
[62] R. Jin *et al.*, "Photoinduced conversion of silver nanospheres to nanoprisms," *Science*, vol. 294, no. 5548, pp. 1901–1903, 2001.
[63] D. Averitt, D. Sarkar, and N. J. Halas, "Plasmon resonance shifts of au-coated Au 2 S nanoshells: Insight into multicomponent nanoparticle growth," *Phys. Rev. Lett.*, vol. 78, 1997, Art. no. 4217.
[64] M. I. Mishchenko, "Light scattering by randomly oriented axially symmetric particles," *J. Opt. Soc. Amer. A*, vol. 8, pp. 871–882, 1991.
[65] M. I. Mishchenko, L. D. Travis, and D. W. Mackowski, "T-matrix computations of light scattering by nonspherical particles: A review," *J. Quant Spectrosc. Radiat. Transf.*, vol. 55, pp. 535–575, 1996.
[66] E. M. Purcell and C. R. Pennypacker, "Scattering and absorption of light by nonspherical dielectric grains," *Astrophys. J.*, vol. 186, pp. 705–714, 1973.
[67] P. K. Jain, W. Huang, and M. A. El Sayed, "On the universal scaling behavior of the distance decay of plasmon coupling in metal nanoparticle pairs: A plasmon ruler equation," *Nano Lett.*, vol. 7, no. 7, pp. 2080–2088, 2007.
[68] L. Gunnarsson *et al.*, "Confined plasmons in nanofabricated single silver particle pairs: Experimental observations of strong interparticle interactions," *J. Phys.Chem. B*, vol. 109, no. 3, pp. 1079–1087, 2005.
[69] A. M. Funston *et al.*, "Plasmon Coupling of Gold Nanorods at Short Distances and in Different Geometries," *Nano Lett.*, vol. 9, no. 0, p. 1651, 2009.
[70] P. K. Jain, W. Huang, and M. A. El Sayed, "On the universal scaling behavior of the distance decay of plasmon coupling in metal nanoparticle pairs a plasmon ruler equation," *Nano Lett.*, vol. 7, no. 7, pp. 2080–2088, 2007.
[71] P. K. Jain, S. Eustis, and M. A. El Sayed, "Plasmon coupling in nanorod assemblies: optical absorption, discrete dipole approximation simulation, and exciton-coupling model," *J. Phys. Chem. B*, vol. 110, no. 37, pp. 18243–18253, 2006.